Supporting Information

Thermo-Mechanically Responsive Crystalline Organic Cantilever

Madushani Dharmarwardana,[a] Raymond P. Welch,[a] Sunah Kwon,[b] Victoria K. Nguyen,[a] Gregory T. McCandless,[a] Mohammad A. Omary,[c] and Jeremiah J. Gassensmith[a] *

[a]Department of Chemistry and Biochemistry, University of Texas at Dallas, 800 West Campbell Road, Richardson, TX 75080-3021; [b]Department of Material Science and Engineering, University of Texas at Dallas, 800 West Campbell Road, Richardson, TX 75080-3021; [c]Department of Chemistry, University of North Texas, 1155 Union Circle, Denton, TX 76203.

Email: gassensmith@utdallas.edu

Contents

Materials

All the chemicals and solvents used for the synthesis and crystallizations (1,4,5,8-naphthalenetetracarboxylic dianhydride, 4-butoxyaniline, N,N-dimethylformamide, chloroform, tetrabutylammonium bromide, chloroform-d) were purchased from Sigma Aldrich.

Instrumentation

Nuclear Magnetic Resonance (NMR)

NMR spectra were measured using a Bruker AVANCE III 500 MHz spectrometer in $CDCl_3$ with $Si(CH_3)_4$ used as reference standard.

Single Crystal X-Ray Diffraction (SXRD)

SXRD data were collected for the two BNDI polymorphs, α-phase and β-phase using a Bruker Kappa D8 Quest diffractometer. Bruker Kappa D8 Quest diffractometer is equipped with an Incoatec microfocus Mo Kα radiation source, HELIOS multilayer optics, Oxford Cryosystems cryostream, and a Photon 100 CMOS detector. Bruker SAINT was used for all data sets for integration and scaling, SADABS was used for absorption correction (multi-scan) and analysis of systematic absences of hkl reflections and XPREP was used for space group selection. All initial triclinic and monoclinic models of the two polymorphs were generated with SHELXT (intrinsic phasing method)[1] and least-squares refinement was carried out with SHELXL2014.[2]

Temperature-dependent Powder X-Ray Diffraction (PXRD)

Temperature-dependent PXRD was collected using a Rigaku Ultima III XRD equipped with an HT 1500 high temperature attachment with Cu Kα radiation. Samples were placed on the sample holder, and measured with 2θ range from 3–40° in a nitrogen gas environment. The temperature of the experiment was programmed from room temperature to 493 K with 10 min equilibration time and 10 K/min heating rate. PXRD data were collected while the sample was heating to 493 K and cooling the sample to room temperature under nitrogen gas.

Thermal Analysis

Thermal properties of BNDI samples were analyzed with differential scanning calorimetry (DSC) using a TA Instruments Q2000. The samples were heated from 200 K to 500 K at a heating rate of 10 K/min, under a flow of nitrogen (50 mL/min).

Hot-stage Polarized Optical Microscopy

Thermo-mechanical behavior was analyzed using a MEIJI TECHNO ML9000 series polarizing microscope equipped with an Instech hot stage. The maximum temperature that the sample can be heated on this stage is 473 K. The sample was placed on a 1 mm thick glass slide and it was heated to 423 K. The actual temperature of the stage was determined by a Phidget Temperature Sensor (P/N 1051_2). After the phase transition, the sample was cooled by sending cooled nitrogen gas through the stage.

Quantification of thermo-mechanical effect

1.5 mm – 4.0 mm sized BNDI crystals were picked using a microscope and one end of the crystal was glued to the 1 mm glass cover slide. Then, a metal ball (4.1 mg steel or 1 mg tungsten carbide)

was glued to the other end of the crystal. The cover slide with this BNDI cantilever was placed on the hot stage, heated to about 473 K, and monitored using a microscope which was placed perpendicular to the crystal. The angle of the BNDI cantilever before and after the phase transition was measured using the MU300 microscope software (AmScope, Irvine, California, USA).

Synthesis and Characterization

Synthesis of BNDI

Butoxyphenyl N-substituted naphthalene diimide (BNDI) was prepared as shown in **Scheme S1**. A mixture of 1,4,5,8-naphthalene-tetracarboxylic dianhydride (NDA) (0.8045 g, 3.000 mmol) and *p*-butoxyaniline (0.9914 g, 6.000 mmol) in DMF (20 mL) was heated under reflux at 110 °C for 24 hours. When the reaction mixture cooled to room temperature, a crystalline solid precipitated, which was collected by filtration as an orange crystalline solid with a 70% yield. ^{1}H–NMR (500 MHz, $CDCl_3$, ppm) (**Figure S1**): 1.01 (t, 7.0 Hz, 6 H), 1.54 (tq, 3.8, 7.2 Hz, 4 H) 1.82 (tt, 6.5, 8.0 Hz, 4 H), 4.04 (t, 4 H, 6.5 Hz) 7.07 (d, J= 8.5 Hz, 4 H) 7.23 (d, 8.5 Hz, 4 H) 8.82 (s, 4 H). ^{13}C–NMR (125 MHz, $CDCl_3$, ppm) (**Figure S2**): 13.88, 19.30, 31.31, 67.99, 115.41, 126.70, 127.08, 127.19, 129.36, 131.43, 159.59, 163.24.

Growth of the α-phase Single Crystals for SXRD

Crude BNDI solid (0.056 g, 1.0 mmol) was placed in a scintillation vial and dissolved in 2.0 ml of $CHCl_3$. The solution was boiled until the solid particles disappeared. The resultant solution was loosely covered with a lid and kept for 2-3 days until crystals appeared.

Growth of the β-phase Single Crystals for SXRD

Crude BNDI (0.056 g, 1.0 mmol) and tetrabutylammonium bromide (0.064 g, 2.0 mmol) were mixed in a scintillation vial and 2.0 ml of $CHCl_3$ was added. The resulting solution was boiled until the solid particles disappeared. The resultant solution was loosely covered with a lid and kept for 2-3 days until crystals appeared.

Single Crystal X-Ray Structure for α-phase and β-phase

Crystallographic data for the α-phase and β-phase have been submitted to the Cambridge Crystallographic Data Center with deposition number CCDC 1497526 and CCDC 1497523, respectively.

SXRD data for α-phase: Blade shape yellow crystal (0.84 × 0.14 × 0.10 mm^3) was used for the SXRD analysis, $C_{34}H_{30}N_2O_6$, M = 592.29, F(000) = 592, Monoclinic, a = 5.026(2), b = 33.756(5), c = 7.9533(14), α = 90°, β = 99.997(10)°, γ = 90°, V = 1328.9(6) Å^3, T = 100 K, Space group $P2_1/c$, Z = 2, D_x = 1.406 gcm^{-3}, 16317 measured reflections, 4061 independent reflections, 3266 reflections with $I > 2\sigma(I)$, $R[F^2 > 2\sigma(F^2)] = 0.050$, $wR(F^2) = 0.138$, S = 1.029, $R_{int} = 0.045$

SXRD data for β-phase: blade shape orange color crystal (0.30 × 0.14 × 0.08 mm^3) was used for SXRD analysis, $C_{34}H_{30}N_2O_6$, M = 592.29, F(000) = 296, Triclinic, a = 4.1636(8), b = 8.1371(18), c = 20.104(5), α = 100.182(11)°, β = 93.124(14)°, γ = 94.102(14)°, V = 667.1(3) Å^3, T = 100(2) K, Space group $P\bar{1}$, Z = 1, D_x = 1.400 gcm^{-3}, 23801 measured reflections, 4086 independent reflections, 2918 reflections with $I > 2\sigma(I)$, $R[F^2 > 2\sigma(F^2)] = 0.052$, $wR(F^2) = 0.136$, S = 1.05, R_{int} = 0.060

Figures and Tables

Table S1: Comparison of crystallographic parameters before and after phase transition

		α-phase	β-phase	Before phase transition	After phase transition
Temperature/ K		100	100	298	100
Crystal System		monoclinic	triclinic	monoclinic	triclinic
Space group		$P2_1/c$	$P\bar{1}$	$P2_1/c$	$P\bar{1}$
Unit cell/ Å	***a*** =	5.026(2)	4.1636(8)	5.092(4)	4.16(1)
	b =	33.756(5)	8.1371(18)	33.62(2)	8.18(2)
	c =	7.9533(14)	20.104(5)	8.148(5)	20.21(5)
	α =	90°	100.182(11)°	90°	100.10(5)°
	β =	99.997(10)°	93.124(14)°	100.11(2)°	93.03(6)°
	γ =	90°	94.102(14)°	90°	94.16(6)°
Volume/ Å^3		1328.8(6)	667.1(3)	1373(2)	675(3)
Crystal color		yellow	red/orange	yellow	red/orange
Z		2	1	2	1

Table S2: Changes of the α-phase BNDI crystal dimension with respect to temperature of three individual crystals[a]

Temperature/ K	Crystal 1		Crystal 2		Crystal 3	
	Length/mm	Width/mm	Length/mm	Width/mm	Length/mm	Width/mm
298	1.509	0.094	1.604	0.105	1.957	0.073
323	1.508	0.095	1.607	0.103	1.961	0.075
383	1.514	0.094	1.616	0.106	1.966	0.075
393	1.418	0.088	1.498	0.098	1.814	0.071
373	1.417	0.086	1.486	0.103	1.816	0.068
323	1.370	0.094	1.423	0.101	1.753	0.069
298	1.340	0.094	1.408	0.097	1.736	0.063

[a]We have only considered the length and width of the crystal.

Table S3: Velocity of expansion of BNDI crystals during the transition from the α-phase to the β-phase (the same three crystals listed in **Table S2**)

Δl/ mm	Δt/ s	Velocity of expansion Δl /Δt (μms^{-1})
0.096	24.48	3.921
0.118	24.76	4.765
0.152	19.95	7.619
Average velocity/ (μms^{-1})		5.535(±1.938)

Table S4-A: Quantitative & qualitative comparison of the mechanical property with the state-of-the-art materials

Reference	Material	Mechanical property	Reversible	Speed of the phase transition	Expansion or contraction of the unit cell parameters upon phase transition
This work[a]	Butoxyphenyl N-substituted naphthalene diimide (Organic)	Primarily bending. Also splitting, jumping, cracking	No	Several Seconds	$a \approx -20\%$ $b \approx -75\%$ $c \approx +150\%$ Average velocity of expansion of the crystal during phase transition = 5.435 μms^{-1}
3	Co-crystals of coronene and 1,2,4,5-tetracyanobenzene (Organic)	Self-healing behavior	Yes	Several seconds	—
4	PHBH[b] (Organic)	Thermosalient effect (jumping) followed by colossal expansion	No	Few milliseconds	$a = +8.8\%$ $b = +12.3\%$ $c \approx -15\%$
5	L-pyroglutamic acid (Organic)	Thermosalient effect (jumping) followed by colossal expansion	No	0.2 milliseconds	α→β L-PGA $a = +1.58\ \%$ $b = -1.57\%$ $c = -0.55\%$ D-PGA $a = +1.66\ \%$ $b = -1.35\%$ $c = +0.57\%$
6	DCBFN[c] (Organic)	Thermosalient effect	No	Few milliseconds	$a = +5.88\%$ $b = +1.5\%$ $c = -2.5\%$
7	Amphiphiles containing tetra(ethylene glycol) moieties (Organic)	Bending	Yes	Several seconds	$a = +2.6\%$ $b = +0.68\%$ $c = -1.2\%$
8	TBB[d] (Organic)	Thermosalient effect	No	Few milliseconds	$\Delta a = -0.323$ Å $\Delta b = +0.475$ Å $\Delta c = +0.052$ Å
9	Oxitropium	Thermosalient	No	10^{-7} s	a = —

	bromide (Organic)	effect (Jumping)			b = 10% c = 8%
10	PPHA[e]	Colossal expansion and thermosalient effect (Jumping)	No	Few milliseconds	Average velocity of expansion of crystal during the phase transition = 0.0418 ms^{-1}

[a]We have calculated changes of the unit cell parameters before and after the phase transition. However, as shown in **Figure 2**, there is a dramatic change in the molecular packing and the symmetry of the crystal structure is not preserved. Thus, interpreting changes of unit cell parameters before and after the phase transition should be done with caution.
[b]PHBH = N′-2-propylydene-4-hydroxybenzohydrazide
[c]DCBFN = 2,6-dichlorobenzylidine-4-fluoro-3-nitroanilin
[d]TBB = 1,2,4,5-tetrabromobenzene
[e]PPHA = (phenylazophenyl)palladium hexafluoroacetylacetonate

Table S4-B: Quantitative comparison of the mechanical property with the state of the art materials

Reference	Velocity/ ms^{-1}	ΔDisplacement	Energy/ μJ	Force/ mN
This work	—	243.4 μm with the 4.1 mg steel ball	0.01	0.04
3	—	—	—	—
4	0.2-0.8	Several mm to cm	—	—
5	0.427	19430 μm	≈ 0.651988	
6	—	—	—	—
7	—	≈ 47.1 μm	—	—
8	—	Several cm	—	—
9	103	Several cm	—	—
10	α→γ= 0.54 γ→β = 4.34×10^{-5}	—	—	—

Table S5: Work done by the BNDI cantilever with different crystal lengths

Reference Figure	Crystal Length/ μm	ΔAngle/ °	Mass lifted/ mg	ΔHeight/ μm	Work Done/ μJ
S12	1120	15	4.113	289.8	0.01164
S13	1476	11	4.113	281.6	0.01131
S14	3055	8	4.113	425.2	0.01708
S15	3489	4	4.113	243.3	0.00977
S16	1632	30	1.667	816.0	0.01599
5	3307	11	0.832	631.0	0.00618
S17	1407	25	0.832	594.6	0.00582

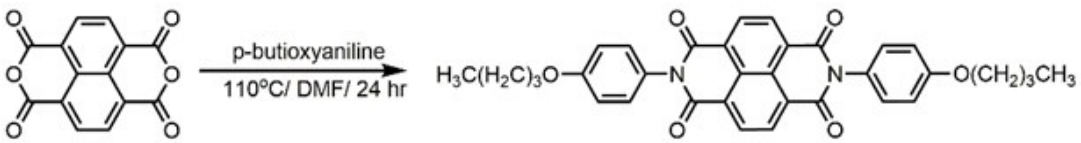

Scheme S1: Synthesis of BNDI

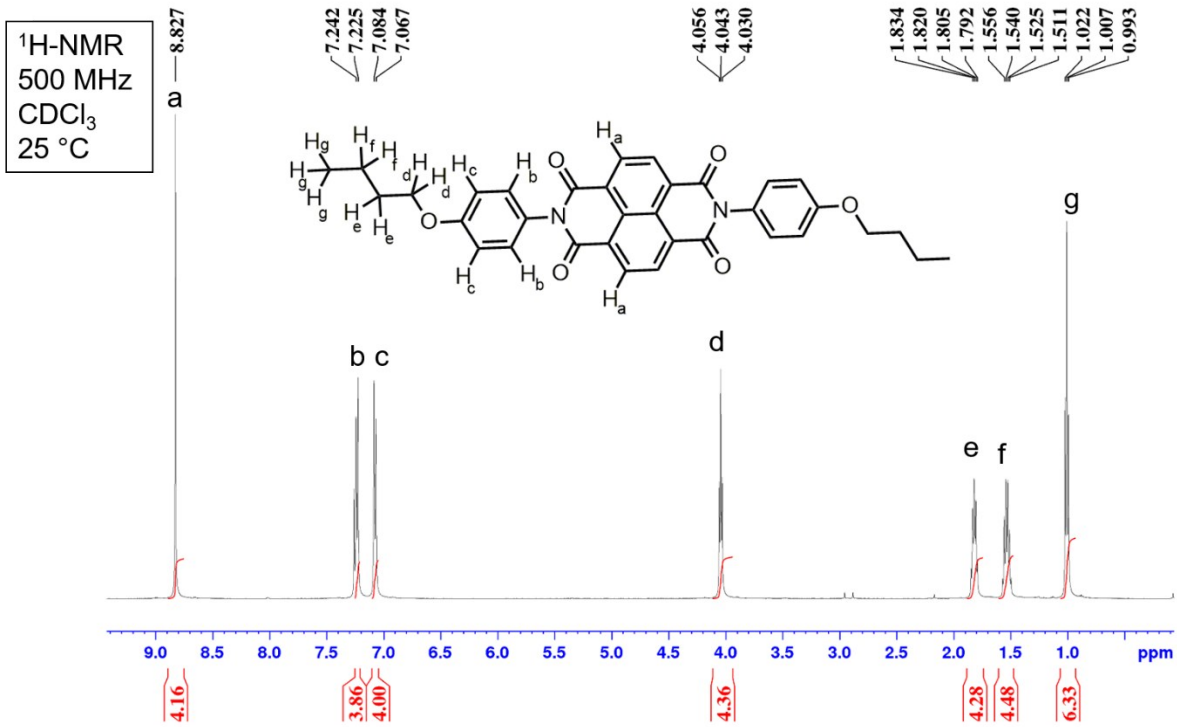

Figure S1: ^{1}H-NMR spectrum of BNDI

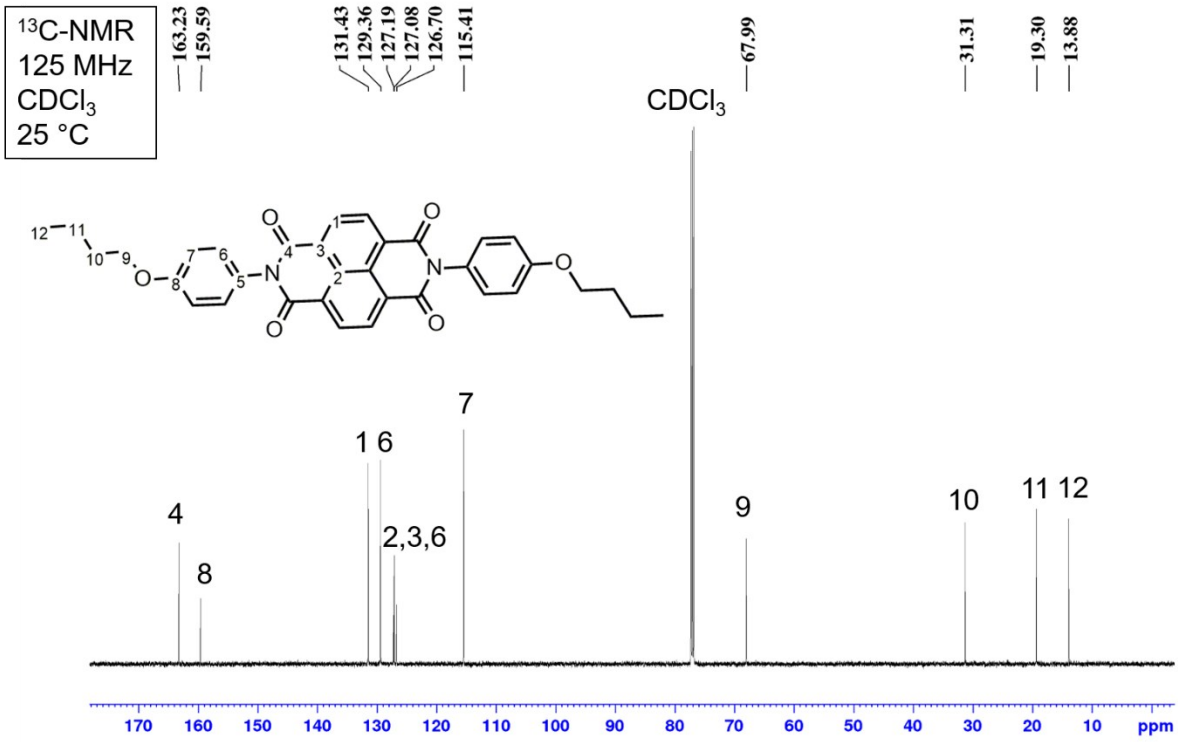

Figure S2: ^{13}C-NMR spectrum of BNDI

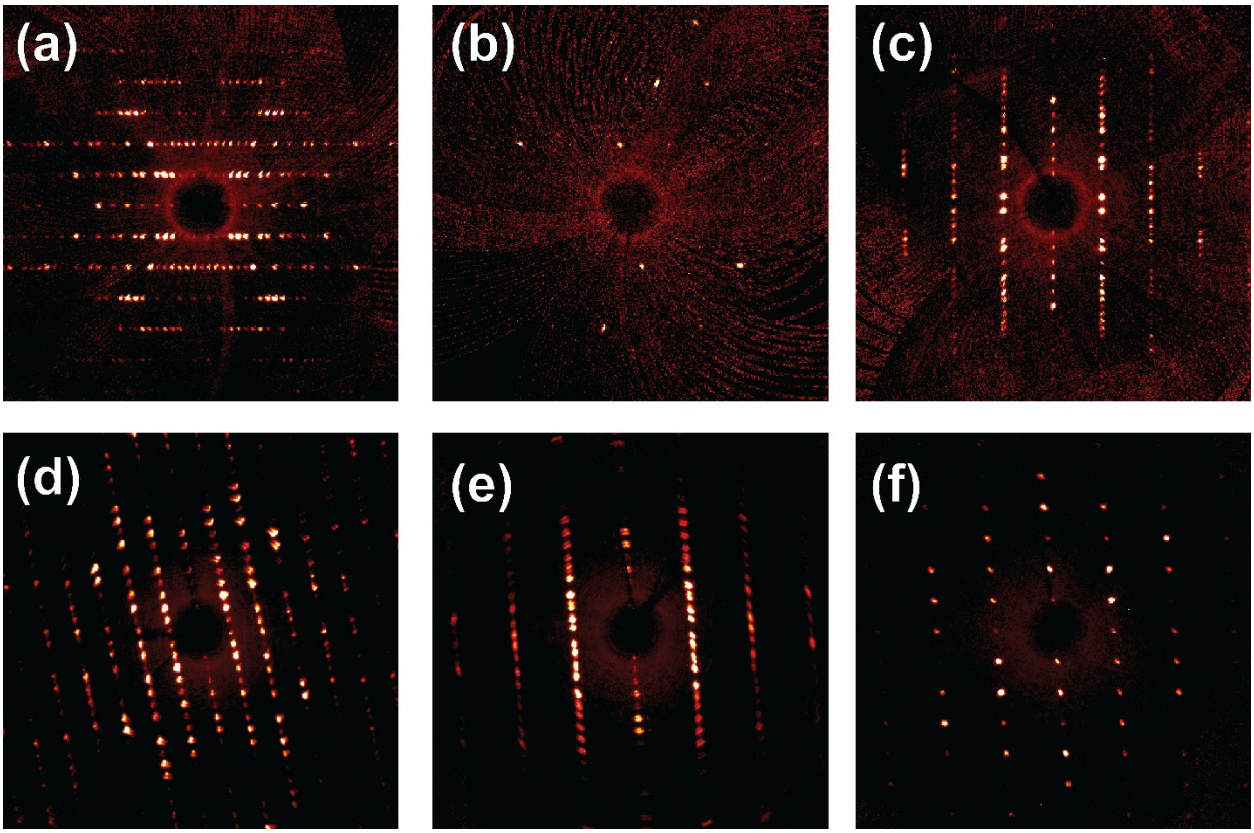

Figure S3: Single crystal diffraction data for α-phase to β-phase transition; Precession images (hk0, h0l, and 0kl) for before (a, b, c) and after (d, e, f) α-phase to β-phase transition. As shown in the (a, b, c) images, the α-phase shows strong diffraction spots in all directions. After the phase transition, the crystal still strongly diffracted and the unit cell parameters were successfully determined. However, as shown in the (d, e, and f) images, weak diffraction spots were observed indicating the emergence of more than one crystalline domain.

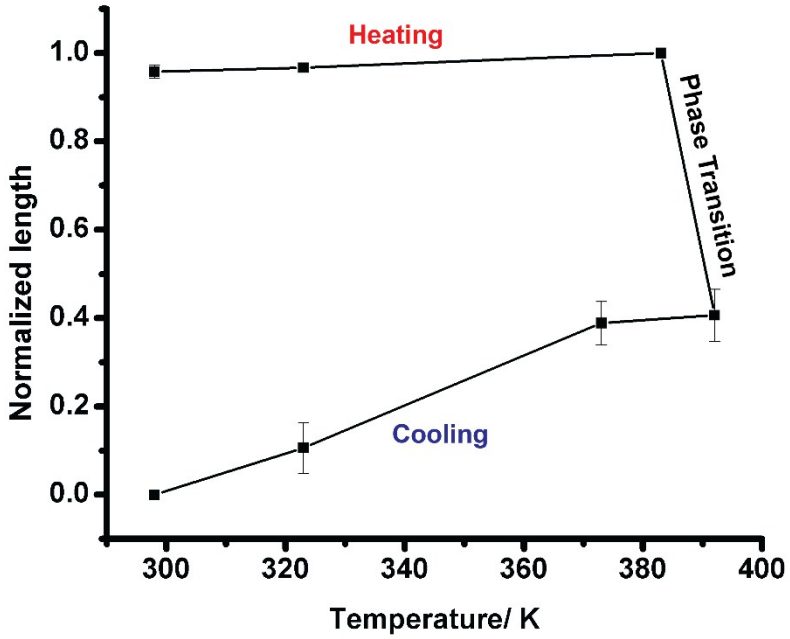

Figure S4: Changes of the crystal length with respect to the temperature. Some error bars are too small to be visible at this scale.

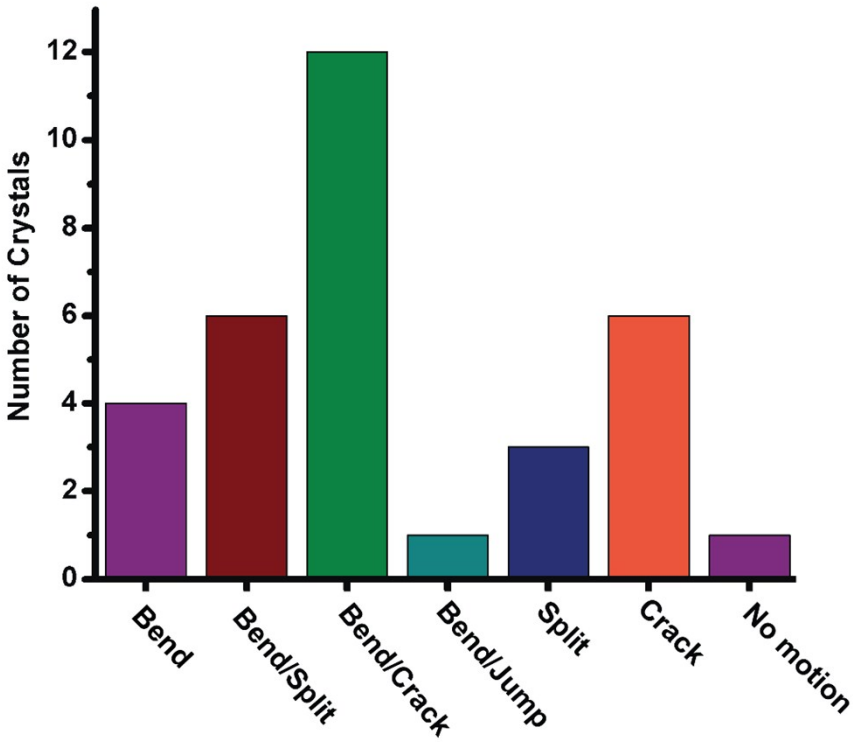

Figure S5: Different thermo-mechanical effects exerted by the BNDI crystals with respect to temperature changes. Total number of crystals used in this graph is 33.

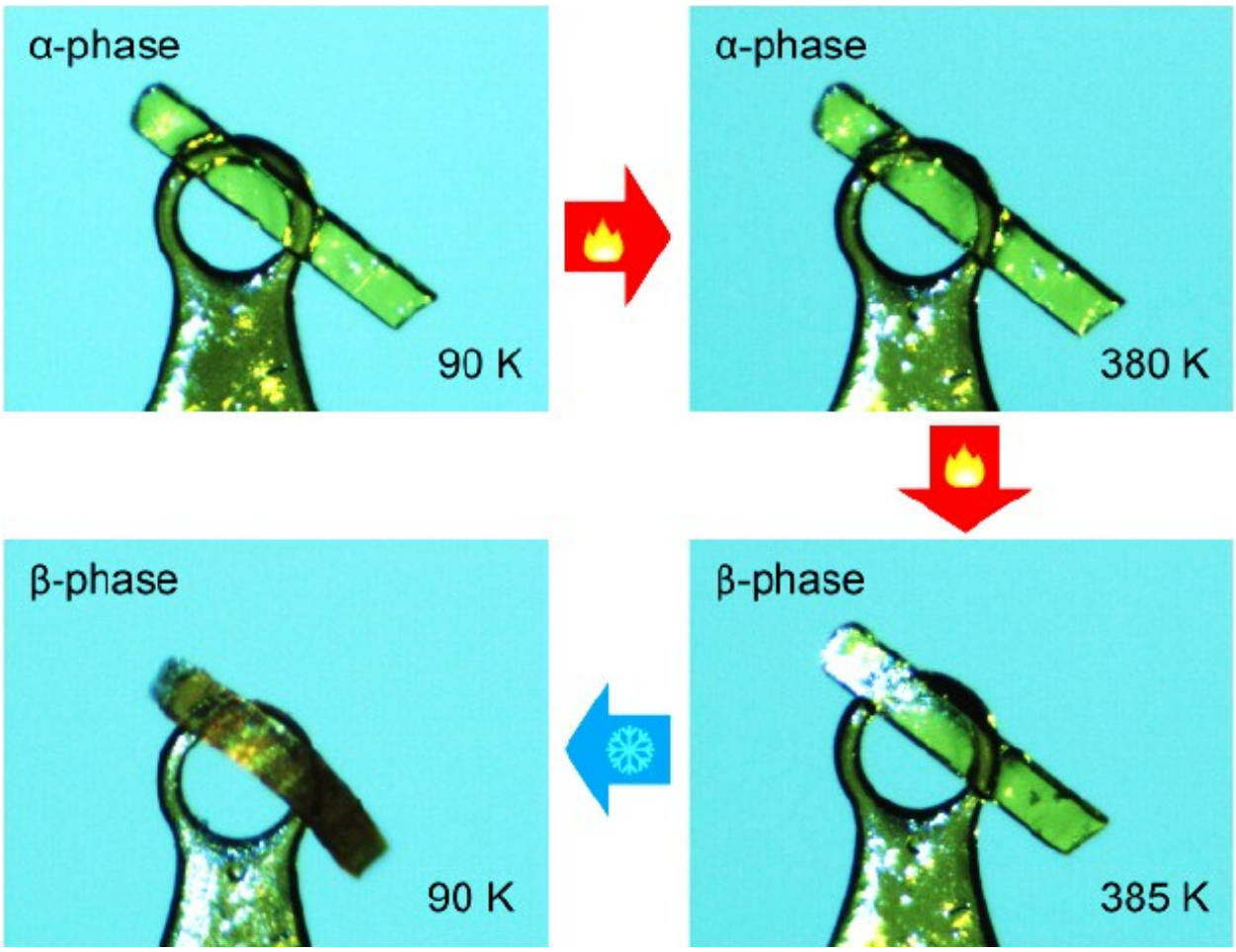

Figure S6: SC-SC phase transition of α-phase to β-phase. Images were taken when the crystal was mounted on a loop for SXRD. The yellow color α-phase started bending as the temperature increased to 385 K due to the phase transition from the α-phase to the β-phase. As the temperature decreased to 90 K using the cryostream, the bending of the single crystal was more obvious due to the shrinking of the unit cell of β-phase, and the crystal converted to a red/range color.

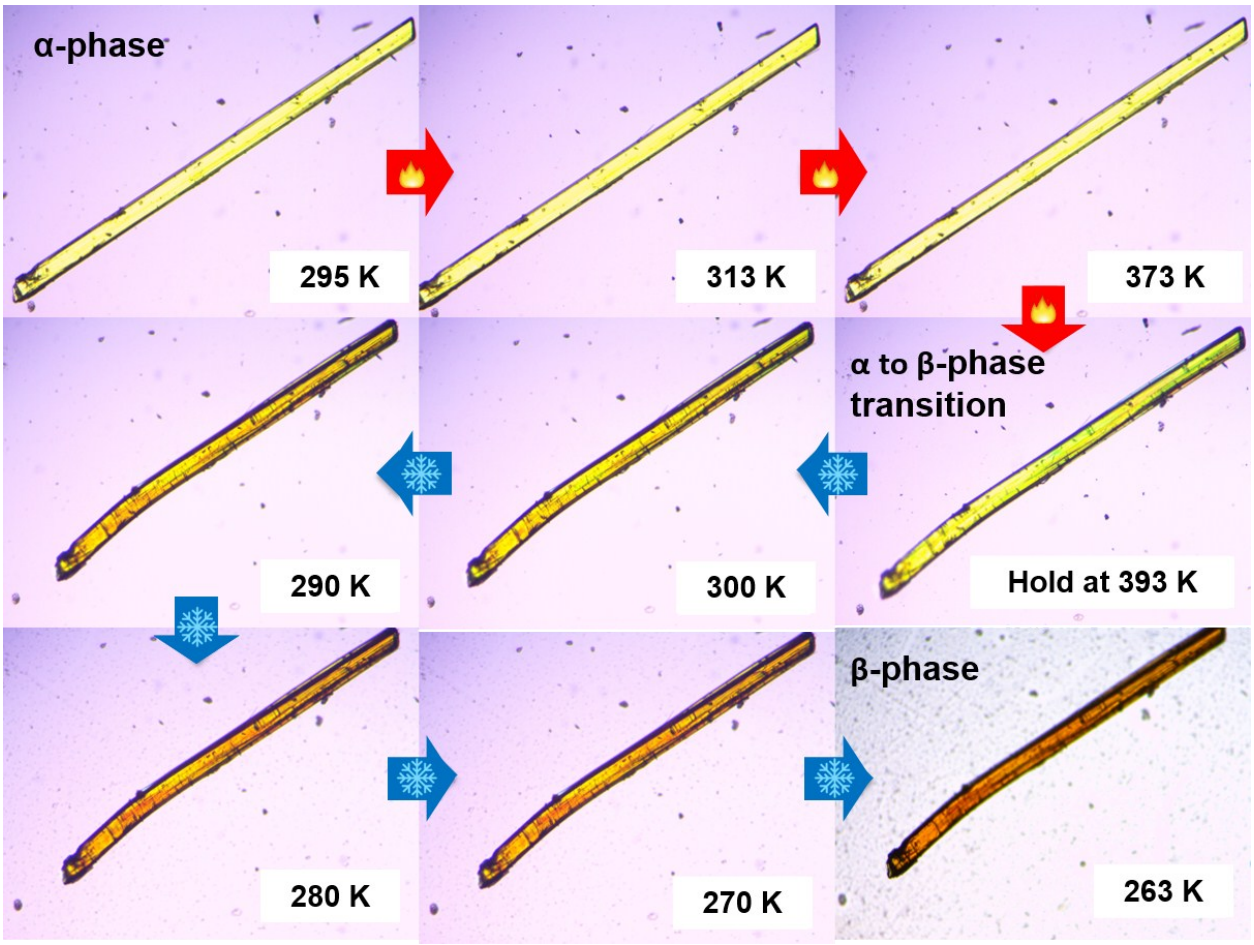

Figure S7: Polarized optical micrographs of α-phase upon heating and cooling. The crystal was placed on a 1 mm think glass slide on the heating stage and the changes of morphology and color were recorded as the crystal was heated continuously beyond the phase transition. At around 373 K, a wave front passed through the crystal and bending of the crystal was observed. Then we cooled the crystal by passing cooled nitrogen gas through the stage. As the temperature decreased, the crystal started changing color from yellow to red/orange because of the α-phase to β-phase transition. The lowest temperature we could achieve from our setup was 263 K. See **Movie S1**.

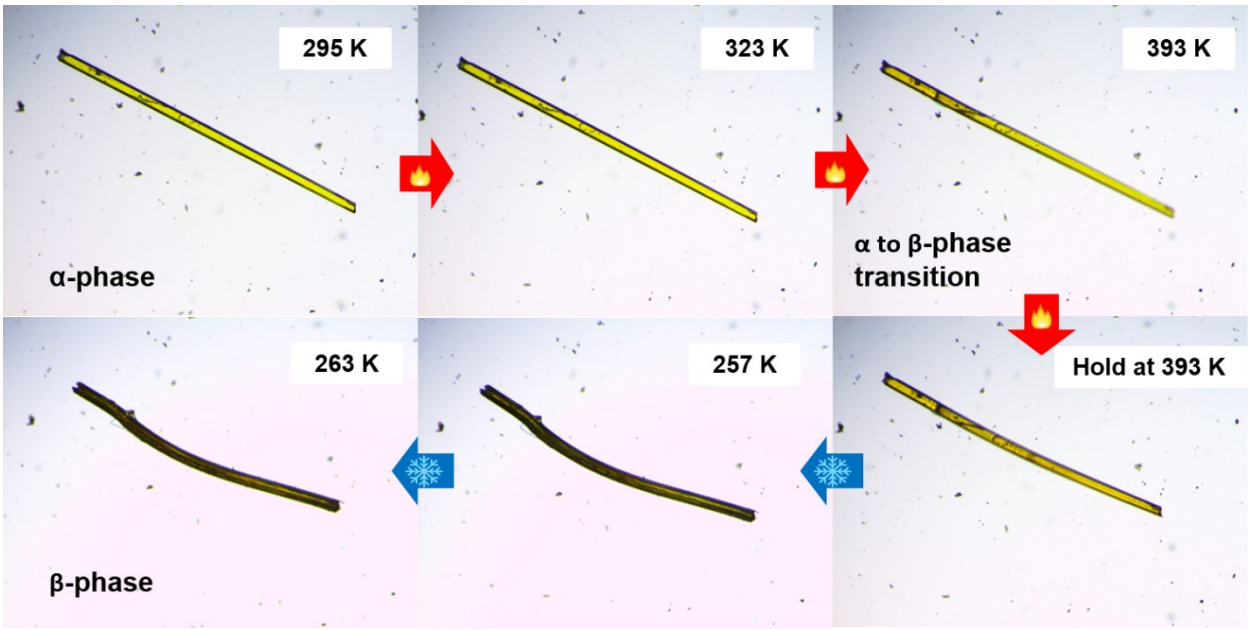

Figure S8: Polarized optical micrographs of α-phase upon heating and cooling. Due to the massive changes in the unit cell dimensions upon the α-phase to β-phase transition the crystal jumped out of the focal plane. See **Movie S2**.

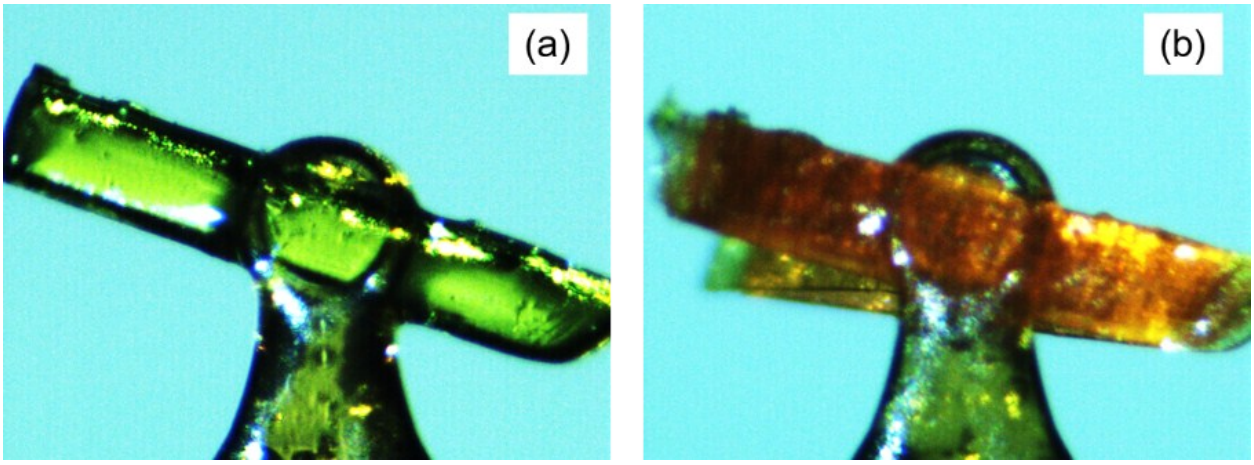

Figure S9: Splitting of single crystals of the α-phase (a) α-phase at 90 K (b) after the α-phase to β-phase transition at 90 K. We mounted an α-phase crystal on a loop for XRD and heated the crystal beyond the phase transition temperature. As we cooled the crystal down to 90 K, the crystal split as a result of the significant structural phase transition.

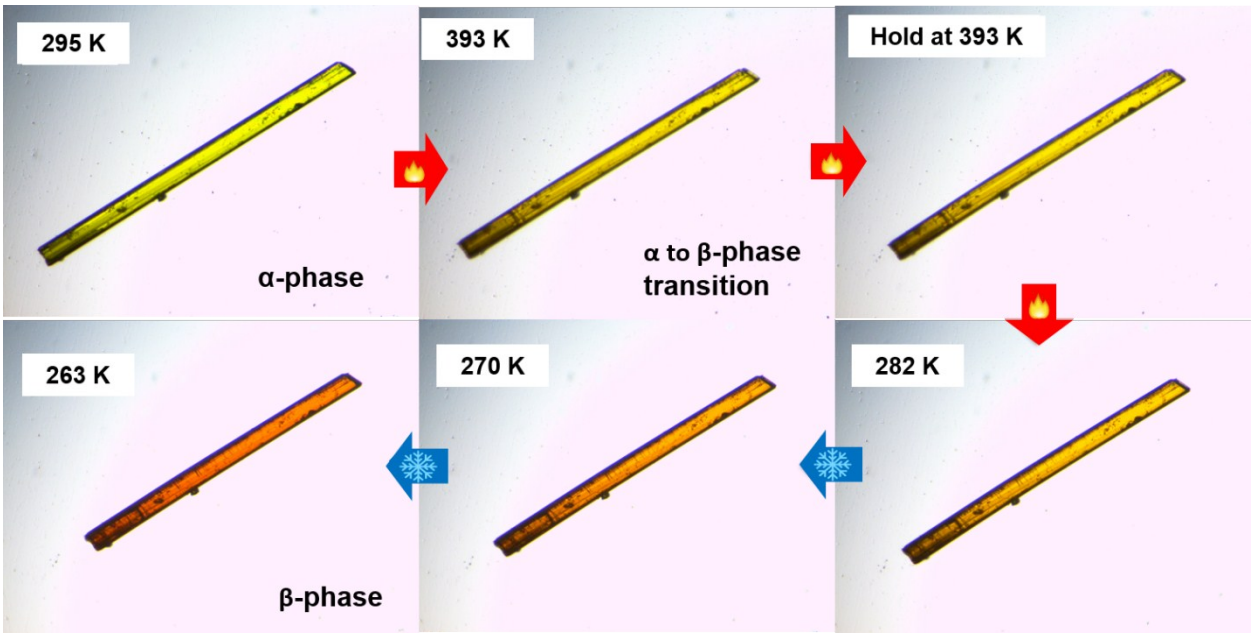

Figure S10: Phase transition of a thick α-phase crystal. When the crystal is thicker compared to the very thin flat crystals, the crystal does not show movement. However, the size of the crystal has been reduced along the long axis as a result of the changes of the unit cell dimensions upon the phase transition. As the stage temperature was reduced, the crystal began showing thermochromic behavior—gradually became red/orange—confirming that the α-phase has been completely transformed to the β-phase.

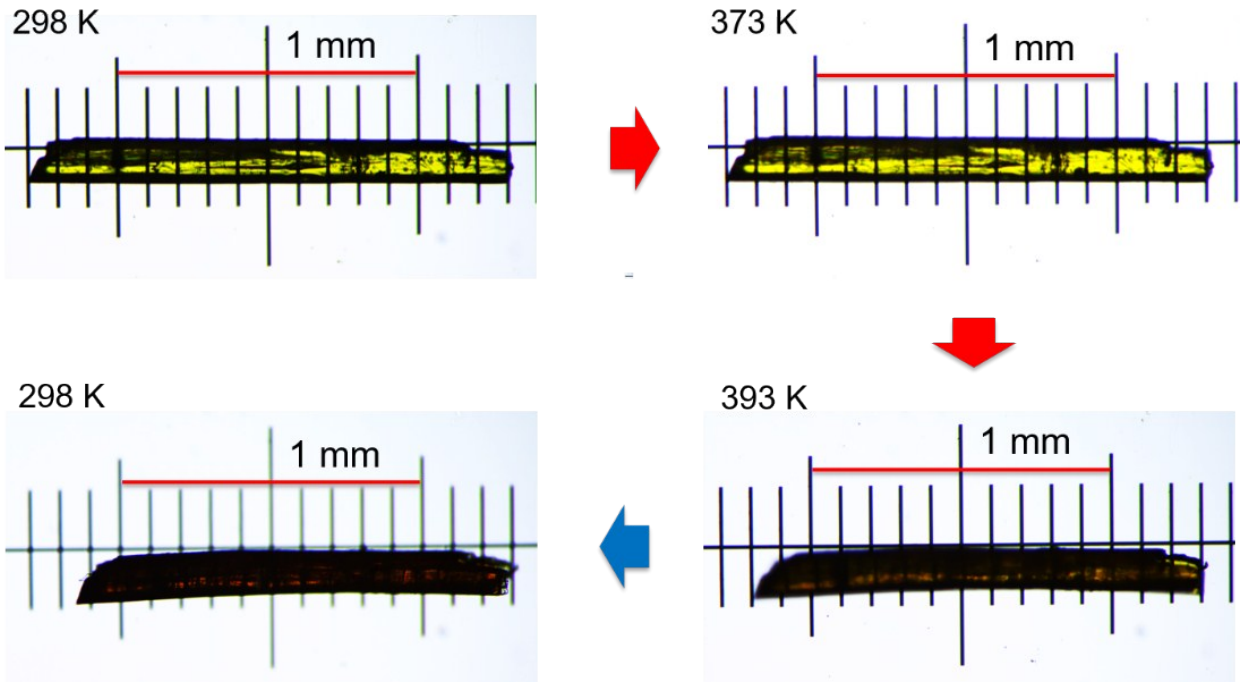

Figure S11: Changes of crystal dimensions upon α-phase to β-phase transition. The crystal was placed on a calibration slide for clarity.

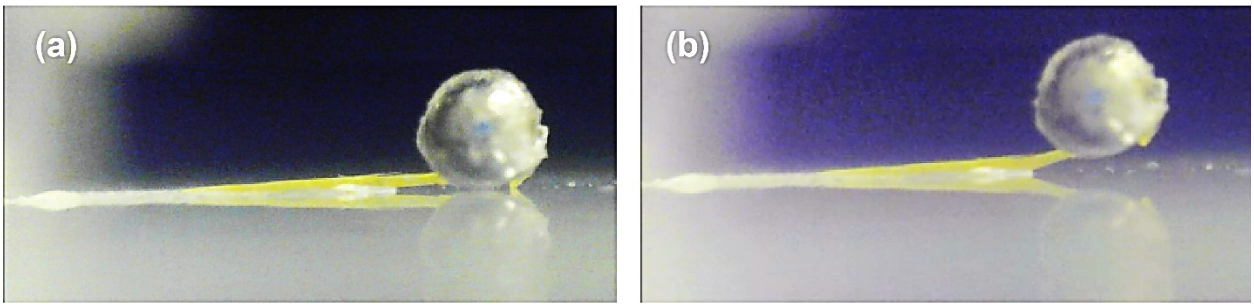

Figure S12: Lifting of a 4.1 mg steel ball by a short BNDI cantilever. The length of the crystal is 1120 μm. See **Movie S4**.

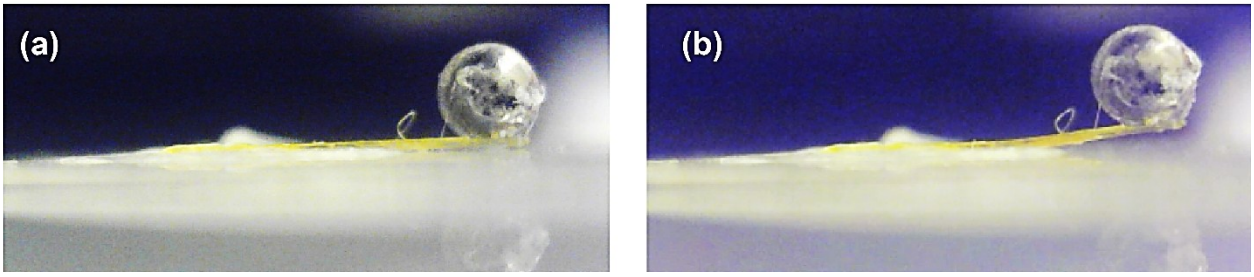

Figure S13: Lifting of a 4.1 mg steel ball by a medium length BNDI cantilever. The length of the crystal is 1476 μm. See **Movie S5**.

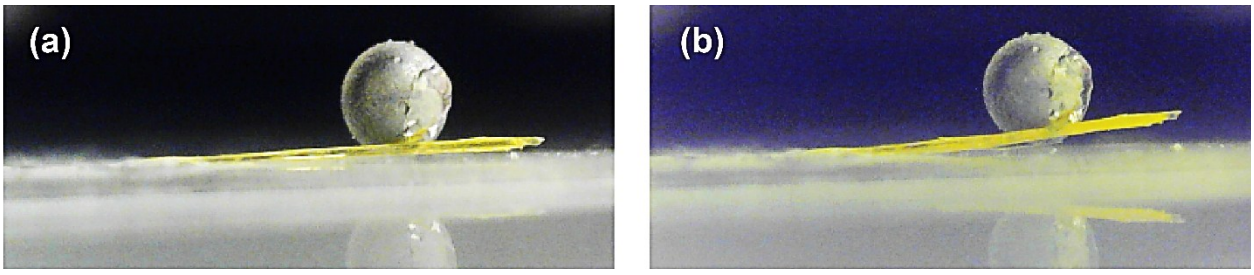

Figure S14: Lifting of a 4.1 mg steel ball by a long BNDI cantilever. The length of the crystal is 3055 μm. See **Movie S6**.

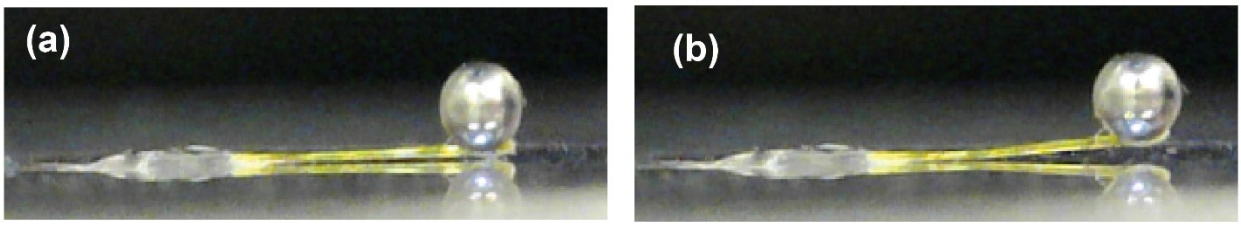

Figure S15: Lifting of a 4.1 mg steel ball by a long BNDI cantilever. The length of the crystal is 3498 μm. See **Movie S7**.

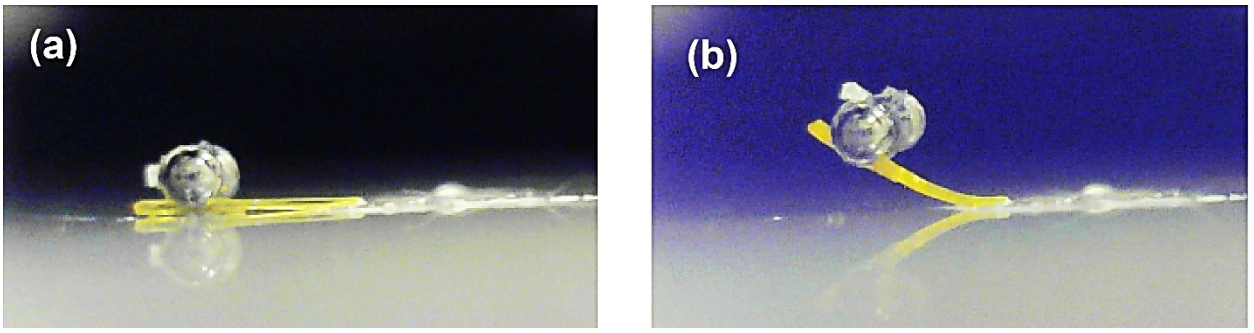

Figure S16: Lifting of two 1 mg tungsten carbide balls by a short BNDI cantilever. The length of the crystal is 1632 μm. See **Movie S8**.

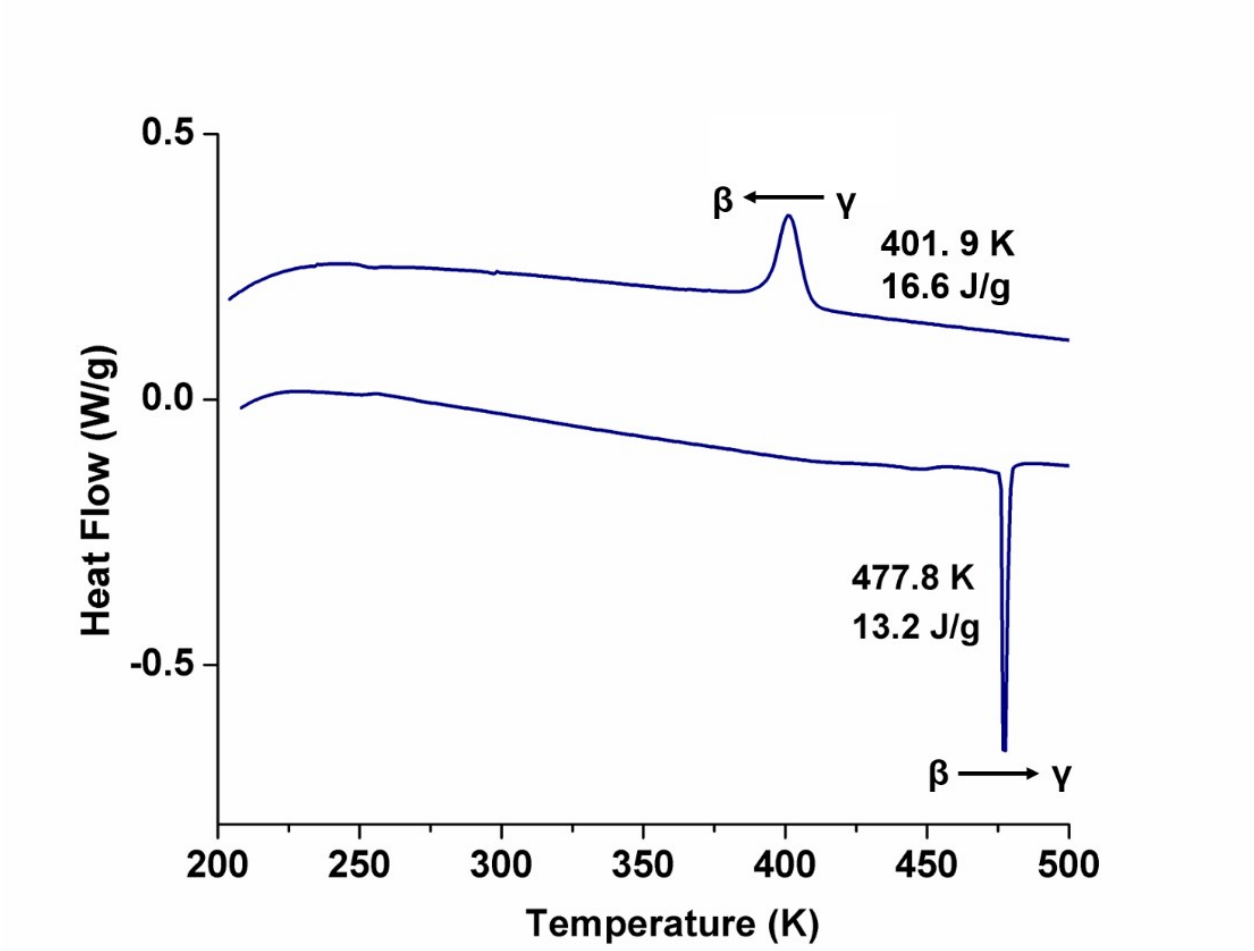

Figure S17: DSC curve for the β-phase; the heating rate is 10 K/min.

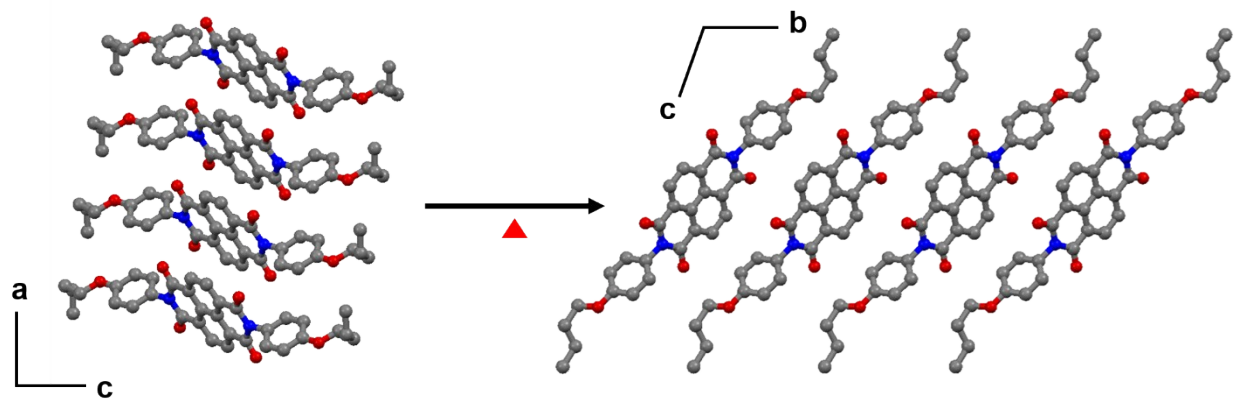

Figure S18: Comparison of packing of the α-phase (*ac* plane) and the β-phase (*bc* plane).

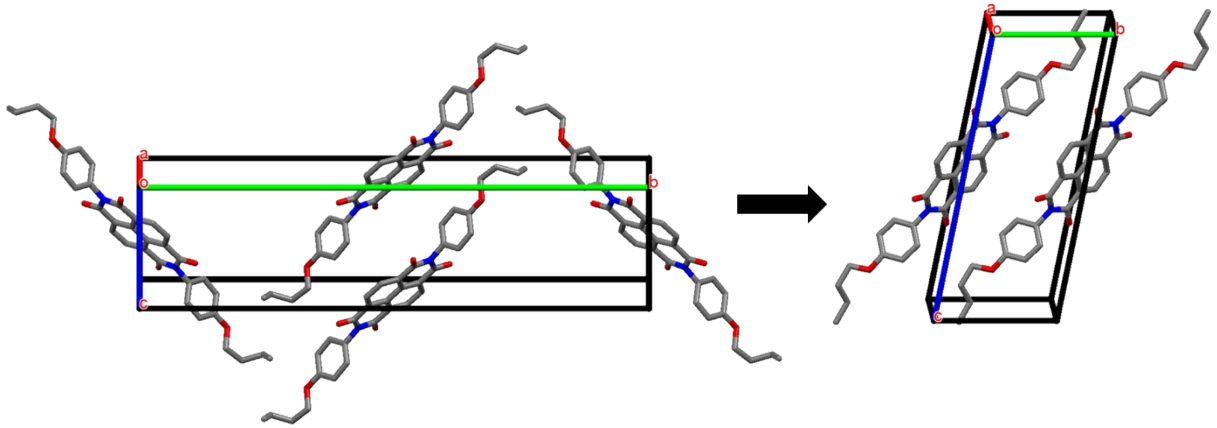

Figure S19: Changes of the unit cell from the α-phase (along *a*-axis) to the β-phase (along *a*-axis).

Search Parameters

During these searches, we mainly focused on whether there are records on thermo-mechanical and thermochromic properties of naphthalene diimides or the perylene diimide family. Additionally, we also looked for compounds that show both thermo-mechanical and thermochromic properties. The search started in August of 2016. The first 20 papers, sorted by relevance, were read for each search term. However, during our search we did not find any record that is similar to the work done in this manuscript.

Google Scholar

"Thermosalient", "Thermosalient naphthalene diimide", "Thermochromic and thermoresponsive", "Thermochromic and Thermo-mechanical naphthalene diimide", "Thermoresponsive naphthalene diimide", "Thermo-mechanical and thermochromic properties of perylene diimide", "Thermo responsive perylene diimide"

Web of Science

"Thermosalient", "Thermosalient naphthalene diimide", "Thermochromic and Thermo-mechanical naphthalene diimide", "Thermoresponsive naphthalene diimide", "Thermo-mechanical and thermochromic properties of perylene diimide", "Thermo-responsive perylene diimide".

References

1. G. M. Sheldrick, *Acta Crystallogr., Sect. A: Found. Adv.*, 2015, **71**, 3-8.
2. G. M. Sheldrick, *Acta Crystallogr., Sect. C: Struct. Chem.*, 2015, **71**, 3-8.
3. G. Liu, J. Liu, X. Ye, L. Nie, P. Gu, X. Tao and Q. Zhang, *Angew. Chem.*, 2017, **56**, 198.
4. M. K. Panda, R. Centore, M. Causa, A. Tuzi, F. Borbone and P. Naumov, *Sci. Rep.*, 2016, **6**, 29610.
5. M. K. Panda, T. Runcevski, A. Husain, R. E. Dinnebier and P. Naumov, *J. Am. Chem. Soc.* 2015, **137**, 1895.
6. S. Ghosh, M. K. Mishra, S. Ganguly and G. R. Desiraju, *J. Am. Chem. Soc.*, 2015, **137**, 9912-9921.
7. T. Shima, T. Muraoka, N. Hoshino, T. Akutagawa, Y. Kobayashi and K. Kinbara, *Angew. Chem.,*, 2014, **126**, 7301.
8. S. C. Sahoo, S. B. Sinha, M. S. Kiran, U. Ramamurty, A. F. Dericioglu, C. M. Reddy and P. Naumov, *J. Am. Chem. Soc.* 2013, **135**, 13843.
9. Z. Skoko, S. Zamir, P. Naumov and J. Bernstein, *J. Am. Chem. Soc.*, 2010, **132**, 14191.
10. M. K. Panda, T. Runcevski, S. C. Sahoo, A. A. Belik, N. K. Nath, R. E. Dinnebier and P. Naumov, *Nat. Commun*., 2014, **5**, 4811.